NeuroImage: Clinical 30 (2021) 102676

Contents lists available at ScienceDirect

NeuroImage: Clinical

journal homepage: www.elsevier.com/locate/ynicl

Brain connectivity during simulated balance in older adults with and without Parkinson's disease

Elizabeth P. Pasman [a], Martin J. McKeown [b], Saurabh Garg [b], Taylor W. Cleworth [c], Bastiaan R. Bloem [d], J. Timothy Inglis [a,e,f], Mark G. Carpenter [a,e,f,*]

[a] School of Kinesiology, University of British Columbia, Vancouver, BC, Canada
[b] Pacific Parkinson's Research Centre, Vancouver, BC, Canada
[c] School of Kinesiology and Health Science, York University, Toronto, ON, Canada
[d] Radboud University Medical Center, Donders Institute for Brain, Cognition and Behaviour, Department of Neurology, Center of Expertise for Parkinson & Movement Disorders, Nijmegen, The Netherlands
[e] Djavad Mowafaghian Centre for Brain Health, University of British Columbia, Vancouver, BC, Canada
[f] International Collaboration on Repair Discoveries, University of British Columbia, Vancouver, BC, Canada

ARTICLE INFO

Keywords:
Brain connectivity
Static balance
Dynamic balance
Parkinson's disease
Postural instability
Elderly

ABSTRACT

Individuals with Parkinson's disease often experience postural instability, a debilitating and largely treatment-resistant symptom. A better understanding of the neural substrates contributing to postural instability could lead to more effective treatments. Constraints of current functional neuroimaging techniques, such as the horizontal orientation of most MRI scanners (forcing participants to lie supine), complicates investigating cortical and subcortical activation patterns and connectivity networks involved in healthy and parkinsonian balance control. In this cross-sectional study, we utilized a newly-validated MRI-compatible balance simulator (based on an inverted pendulum) that enabled participants to perform balance-relevant tasks while supine in the scanner. We utilized functional MRI to explore effective connectivity underlying static and dynamic balance control in healthy older adults ($n = 17$) and individuals with Parkinson's disease while on medication ($n = 17$). Participants performed four tasks within the scanner with eyes closed: resting, proprioceptive tracking of passive ankle movement, static balancing of the simulator, and dynamic responses to random perturbations of the simulator. All analyses were done in the participant's native space without spatial transformation to a common template. Effective connectivity between 57 regions of interest was computed using a Bayesian Network learning approach with false discovery rate set to 5%. The first 12 principal components of the connection weights, binomial logistic regression, and cross-validation were used to create 4 separate models: contrasting static balancing vs {rest, proprioception} and dynamic balancing vs {rest, proprioception} for both controls and individuals with Parkinson's disease. In order to directly compare relevant connections between controls and individuals with Parkinson's disease, we used connections relevant for predicting a task in either controls or individuals with Parkinson's disease in logistic regression with Least Absolute Shrinkage and Selection Operator regularization. During dynamic balancing, we observed decreased connectivity between different motor areas and increased connectivity from the brainstem to several cortical and subcortical areas in controls, while individuals with Parkinson's disease showed increased connectivity associated with motor and parietal areas, and decreased connectivity from brainstem to other subcortical areas. No significant models were found for static balancing in either group. Our results support the notion that dynamic balance control in individuals with Parkinson's disease relies more on cortical motor areas compared to healthy older adults, who show a preference of subcortical control during dynamic balancing.

Abbreviations: DB, dynamic balancing; DBN, dynamic Bayesian network; FDR, false discovery rate; fMRI, functional MRI; fNIRS, functional near-infrared spectroscopy; H&Y, Hoehn and Yahr; LASSO, least absolute shrinkage and selection operator; PC, principal component; PCA, principal component analysis; PCfdr, Peter Spirtes and Clark Glymour, false discovery rate; ROI, region of interest; SB, static balancing; SMA, supplementary motor area; UPDRS-ME, Unified Parkinson's Disease Rating Scale – Motor Examination.

* Corresponding author at: School of Kinesiology, University of British Columbia, Osborne Centre Unit I, 6108 Thunderbird Blvd, Vancouver, BC V6T 1Z4, Canada.
E-mail address: mark.carpenter@ubc.ca (M.G. Carpenter).

https://doi.org/10.1016/j.nicl.2021.102676
Received 6 December 2020; Received in revised form 2 April 2021; Accepted 10 April 2021
Available online 16 April 2021

1. Introduction

Postural instability is a debilitating symptom of Parkinson's disease that is often treatment-resistant and a precursor to falls (Boonstra et al., 2008; Grimbergen et al., 2009; Crouse et al., 2016; Fasano et al., 2017). Effective treatment of postural instability in Parkinson's disease is significantly impeded by a relatively poor understanding of both the neural networks involved in healthy balance and the pathophysiology underlying balance deficits in individuals with Parkinson's disease (Grimbergen et al., 2009; Kim et al., 2013; Crouse et al., 2016). Balance control in healthy individuals likely involves an integrated network of cortical and subcortical structures (Takakusaki, 2017), however, the specific networks involved remain unresolved. Moreover, the extent to which changes in the activation of, and connection between, cortical and subcortical structures contribute to balance deficits in Parkinson's disease has not been established.

Investigating neural activation patterns and connectivity networks contributing to healthy and abnormal balance control is hindered by the constraints of current functional neuroimaging options. Although portable neuroimaging techniques, such as EEG and functional near-infrared spectroscopy (fNIRS), allow for functional neuroimaging in participants standing upright (albeit frequently with unacceptable levels of movement artifact), their ability to record from subcortical structures is limited. Both cortical and subcortical activity can be measured using PET and functional MRI (fMRI) scanners, however, these scanners are almost exclusively horizontal, requiring the participant to be lying supine. Wearable PET scanners have recently been developed (Bauer et al., 2016; Melroy et al., 2017), but are limited by poor temporal resolution and the weight of the wearable PET device, potentially interfering with balance control.

Motor imagery of static and dynamic balance tasks offers a less-than-ideal approach to probing balance networks but has been successfully employed in healthy participants (Malouin et al., 2003; Jahn et al., 2004; Jahn et al.., 2008; Zwergal et al., 2012; Ferraye et al., 2014; Taube et al., 2015; Bhatt et al., 2018; Mouthon et al., 2018; Gilat et al., 2019) and individuals with Parkinson's disease (Peterson et al., 2014; Gilat et al., 2019). Unsurprisingly, some brain areas are more strongly, or selectively, activated during actual motor execution of a task compared to motor imagery of the same task, and *vice versa* (Guillot et al., 2012; O'Shea and Moran, 2017). The ability to perform motor imagery varies greatly among individuals (Saimpont et al., 2015) and declines with age for complex movements (Saimpont et al., 2013; Kalicinski et al., 2015), making it less suitable for investigating balance networks in healthy older participants and individuals with Parkinson's disease.

A few studies have attempted performance of balance-related tasks while recording fMRI data in participants lying supine (Karim et al., 2014; De Lima-Pardini et al., 2017). Karim et al. (2014) constructed an MRI-compatible force platform and had participants use visual feedback to generate anterior-posterior ankle torque using feed-forward volitional control. Likewise, De Lima-Pardini et al. (2017) developed an MRI compatible force measurement system to investigate anticipatory postural adjustments during single leg raises to simulate step initiation. Although these prior studies had participants perform balance-related tasks while lying down, neither truly simulated free-standing balance.

Recently, we developed and validated a novel MRI-compatible balance simulator able to detect postural instability in individuals with Parkinson's disease (Pasman et al., 2019). The balance simulator was shown to be relatively easy to control using muscles around the ankle joint for both healthy participants and individuals with Parkinson's disease after only a few minutes of practice outside the scanner. During validation, lab studies verified that qualitatively similar balance behaviour was seen in participants when maintaining balance of their body during upright standing and when maintaining balance using the balance simulator while supine with the eyes open and eyes closed. The balance simulator was also sensitive enough to detect deficits in both static and dynamic reactive balance control in individuals with Parkinson's disease compared to healthy age-matched participants, independent of vision (Pasman et al., 2019).

Here we use this newly-validated balance simulator during fMRI scanning to investigate effective connectivity during static and dynamic balance control tasks in individuals with Parkinson's disease and healthy older adults. As abnormal brain connectivity patterns have previously been found in individuals with Parkinson's disease at rest and during a variety of motor and non-motor tasks (Filippi et al., 2018), we hypothesized differences in brain connectivity networks between individuals with Parkinson's disease and healthy elderly during performance of simulated free-standing static and dynamic balance tasks.

2. Materials and methods

2.1. Participants

Twenty individuals with Parkinson's disease and 19 age-matched elderly controls, recruited from the community and through the Pacific Parkinson's Research Centre in Vancouver, participated in this study. Exclusion criteria for individuals with Parkinson's disease were any of the following medical issues (self-reported during initial telephone screening): presence of atypical parkinsonism; any prior neurosurgical procedures such as deep brain stimulation; excessive levodopa-induced dyskinesias that impaired their balance; botulinum toxin injections in lower leg muscles within the last 3 months; documented proprioceptive loss (e.g., abnormal vibratory sense, altered joint position sense, etc.); dementia precluding informed consent; history of other neurological disease (e.g., stroke, seizures); and medical issues (other than Parkinson's disease) that influenced their balance. Controls were excluded if during initial phone screening they self-reported any medical conditions that influenced their balance. Participants in both groups were also excluded if they exceeded the height (max height: 182 cm) and weight (max weight participant and balance simulator combined: 136 kg) restrictions of the MRI scanner, and if they had any contraindications precluding them from undergoing MRI scanning. All participants were fluent in English. All participants provided written informed consent prior to testing and followed experimental procedures that were approved by the UBC Clinical Research Ethics Board, the Vancouver Coastal Health Research Institute, and the UBC MRI Research Centre. Data collection took place at the UBC MRI Research Centre from April 2016 until October 2016. Five participants were excluded due to: inability to perform the simulated balancing tasks during the familiarization session in the laboratory ($n = 2$), inability to complete the protocol in the MRI scanner ($n = 2$), and finding of an incidental abnormality on their anatomical MRI scan ($n = 1$). Therefore, 17 individuals with Parkinson's disease and 17 controls were included in the final data set (Table 1).

Individuals with Parkinson's disease were examined approximately one hour after intake of their regular antiparkinson medication to coincide with their subjectively best clinical 'on' condition and specifically assess dopa-unresponsive balance effects. All participants completed a brief balance-oriented medical history survey, including the occurrence of prior falls within the past 6 months. The Hoehn and Yahr

Table 1
Baseline participant characteristics.

	Parkinson	Control	Statistics
General information			
Sample size	17	17	
Age (years)	67.6 (1.1)	68.1 (1.3)	$p = 0.810$
Number of women (%)	8 (47%)	10 (59%)	$p = 0.732$
Height (cm)	168.7 (1.5)	166.2 (2.2)	$p = 0.350$
Weight (kg)	71.2 (3.2)	65.8 (3.7)	$p = 0.282$
Fallers (≤6 months)	4 (24%)	1 (6%)	$p = 0.335$

Data are displayed as mean (SE) or number of persons (percentage between parentheses).

(H&Y) scale (Goetz et al., 2004) and Unified Parkinson's Disease Rating Scale motor examination (UPDRS-ME) (Goetz et al., 2008) were administered to individuals with Parkinson's disease (Table 2). The clinical assessments were done on a separate day prior to MRI scanning (range 0–31 days, mean ± SD 9 ± 8 days) when participants were familiarized, in the laboratory, with the balance simulator and the tasks they would be performing in the MRI scanner.

2.2. Apparatus

During the simulated stance trials participants were asked to control a customized balance simulator ("simulator") (Pasman et al., 2019). Briefly, in the simulator the participant lay supine with their feet placed against a footplate that controlled a free-standing inverted pendulum in the anterior-posterior direction about an axis aligned with the ankle joints (Fig. 1A and 1B). The mass on the simulator was adjusted such that the estimated load stiffness was about 60% of the ankle load stiffness seen during upright quiet stance (range 38–81%, mean ± SD 60 ± 8.7%). Participants controlled the movement of the inverted pendulum by contracting ankle plantar-flexors and dorsi-flexors, similar to the control of upright stance (Billot et al., 2010). To mimic the gravitational force that pulls the body towards the ground during upright stance, participants had tightly-fastened adjustable straps wrapped around the waist and shoulders which were then attached to the base of the simulator and tightened as much as possible without discomfort, to increase the force between the participant's feet and the simulator foot-plate. The straps helped ensure the participant's heels would always remain in contact with the simulator footplate when contracting their plantar-flexor muscles and therefore movement of the simulator could generate relevant sensory input at the foot and ankle (e.g., inputs from joint receptors, Golgi tendon organs, muscle spindles, and foot sole cutaneous receptors) during the simulated stance trials. Mechanical stops were used to limit the simulator to a range of ±17° to ensure participant safety. In addition, the experimenter stood beside the simulator at all times throughout the testing to assist if needed.

2.3. Experimental tasks

Participants performed 4 different tasks: resting, proprioceptive, static balancing (SB), and dynamic balancing (DB). Since Parkinson's disease effects on simulated SB performance were previously found to be independent of vision (Pasman et al., 2019), all tasks were performed with the eyes closed to prevent the activation of cortical regions associated with processing of visual information. The resting and proprioceptive tasks were used as control tasks. During the resting state portion, participants were instructed to remain awake and lay still. During the proprioceptive task, the simulator was moved by the experimenter and participants were instructed to continuously track the passive movement of the ankle joints by moving their left index finger. Using the proprioceptive task as one of the control tasks ensured brain connectivity seen during the balancing tasks was due to balance related activation, not solely proprioception. In the SB task, participants were instructed to keep the simulator as still as possible. In the DB task, participants were instructed to keep the simulator balanced while responding to transient, random, anterior-posterior perturbations applied to the simulator by the experimenter using a hand-held bar.

During the familiarization session in the laboratory, all participants were given the opportunity to practice the proprioceptive, SB, and DB tasks until they felt comfortable. Subsequently, they performed the tasks for 2-minute trials, corresponding to the experimental protocol used during the MRI scanning session (Fig. 1C). Additionally, the height and weight of the participants were measured to ensure the height and weight restrictions of the MRI scanning table would not be exceeded. Finally, participants who were unable to perform the SB and/or DB balancing tasks during the familiarization session were excluded from MRI scanning participation.

During the MRI scanning session, the resting task was performed first (Fig. 1C). The order of the SB and DB tasks was counterbalance across participants, but the proprioceptive task was always presented in between the balancing tasks to minimize fatigue. In addition, we allowed 2 min of rest between each task.

2.4. MRI scanning

MRI data were collected on a 3 Tesla scanner (Philips Achieva 3.0 T R3.2; Philips Medical Systems, The Netherlands) equipped with an 8-channel head-coil. Head motion was minimized by a strap placed around the participant's head within the head coil, and foam wedged between the participant's head and the head coil. Participants wore ear plugs and earmuffs to minimize scanner noise. An MRI safe sandbag was placed on top of the participant's pelvic area to further stabilize the hips during the balancing tasks.

During fMRI scanning, single-shot gradient-echo echo-planar T2*-weighted images with blood oxygenation level-dependent contrast were taken of the whole brain, including the cerebellum and brainstem. Scanning parameters were: repetition time 2000 ms, echo time 30 ms,

Table 2
Clinical characteristics individuals with Parkinson's disease.

PD_{ON}	Age (years)	Disease duration (years)	UPDRS-ME score	Hoehn & Yahr score	Levodopa equivalent dose	Antiparkinson medication
1	68	2	8	1	225	Levodopa/carbidopa
2	72	2	31	2	300	Levodopa/carbidopa
3	74	4	25	2	325	Levodopa/carbidopa, Rasagiline
4	67	3	44	2	850	Levodopa/carbidopa
5	73	6	36	2	900	Levodopa/carbidopa, Rasagiline, Pramipexole
6	60	2	7	1	300	Levodopa/carbidopa
7	61	9	18	2	750	Levodopa/carbidopa
8	64	14	46	3	1150	Levodopa/carbidopa, Pramipexole
9	75	4	31	2	775	Levodopa/carbidopa, Rasagiline
10	70	7	31	3	1450	Levodopa/carbidopa, Rasagiline, Amantadine
11	68	10	20	2	900	Levodopa/carbidopa
12	59	7	19	1	450	Levodopa/carbidopa
13	68	6	20	2	948	Levodopa/carbidopa, Entacapone
14	69	1	34	2	150	Levodopa/carbidopa
15	65	12	16	2	1015	Levodopa/carbidopa, Rasagiline, Ropinirol
16	69	4	28	2	200	Levodopa/carbidopa
17	67	6	39	2	600	Levodopa/carbidopa, Rasagiline
Range	59–75	1–14	7–46	1–3	150–1450	
Mean (SE)	67.6 (1.1)	5.8 (0.9)	26.6 (2.8)	–	664.0 (92.5)	

PD_{ON}, Individuals with Parkinson's disease; Maximum Unified Parkinson's Disease Rating Scale motor examination (UPDRS-ME) score is 108; Maximum Hoehn & Yahr (H&Y) score is 5.

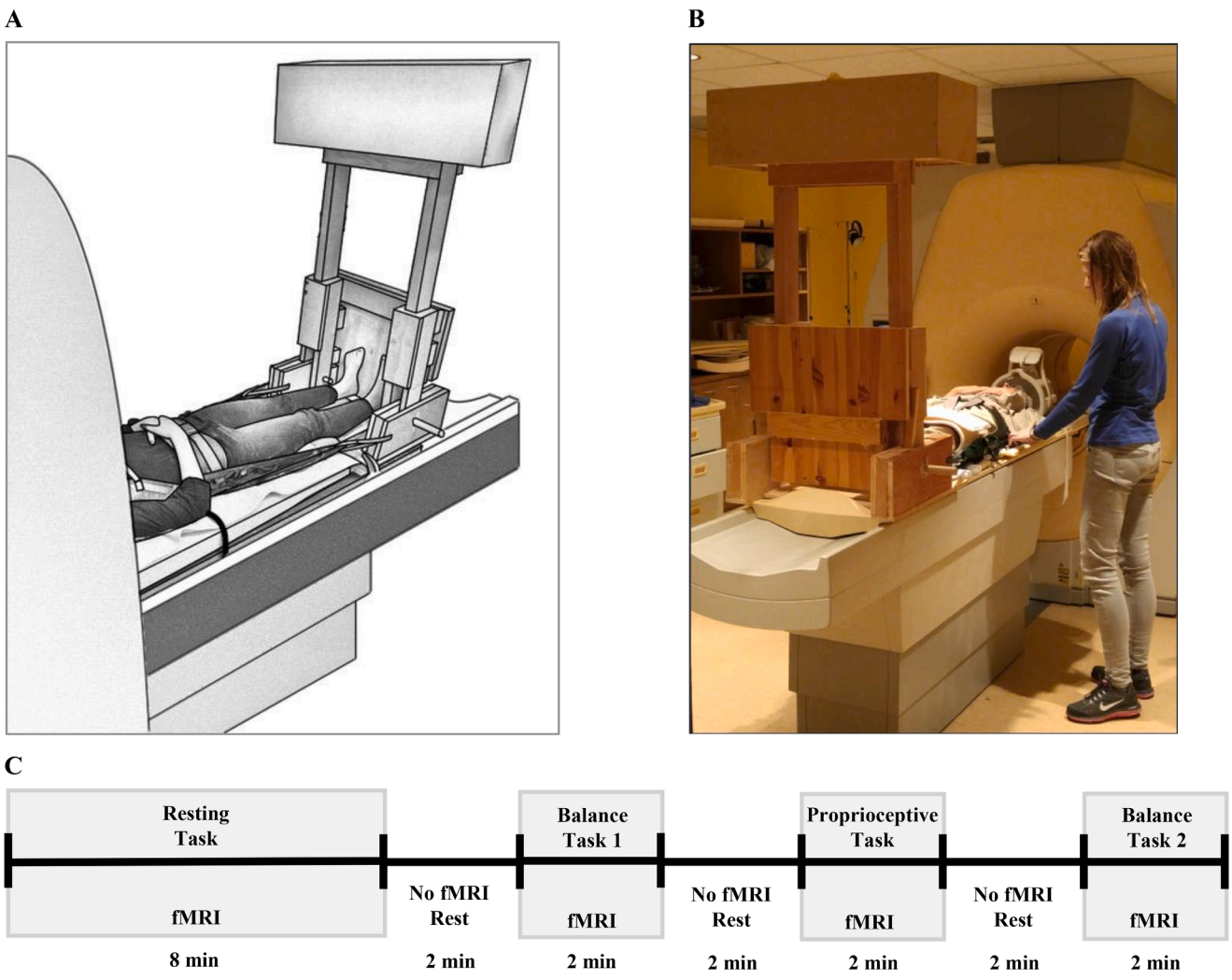

Fig. 1. Experimental set-up of the balance simulator in the MRI environment (A and B), and functional MRI scanning experimental protocol (C) with the order of the static and dynamic balancing tasks counterbalanced across participants and the proprioceptive task always presented in between the balancing tasks.

flip angle 90°, field of view 240 × 240 × 143 mm, matrix size 80 × 80, pixel size 3.0 × 3.0 mm. Thirty-six axial slices of 3.97 mm thickness were collected in each volume, with a gap thickness of 1 mm. A high resolution, 3-dimensional T1-weighted image of the whole brain was acquired, using a multi-shot Turbo Field Echo sequence (repetition/echo time 7.7/3.5 ms; field of view 256 × 200 × 170 mm; matrix 256 × 200; voxel size 1.0 mm^3; 170 axial slices; no fat suppression; scanning time ~ 6.5 min), to facilitate anatomical localization of activation for each participant. The duration of each functional run was 8 min for the resting task and 2 min for the other three tasks.

2.5. Functional MRI preprocessing

The first three volumes from each functional run were discarded for all trials. The fMRI data collected were preprocessed using the AFNI software package. Preprocessing steps performed on the whole brain included despiking, slice time correction, and 3-D isotropic reslicing (3 mm in each dimension). Motion correction using rigid body alignment was performed to correct for any major head motion during scanning. As the brainstem can move independently from the rest of the brain, a separate motion correction of the brainstem was performed. The amount of head motion was assessed using mean volume-to-volume framewise displacement (Power et al., 2012). Fifty-seven regions of interest (ROIs) were defined using FreeSurfer software (Harvard, MA, USA), and HMAT atlas for motor areas (Mayka et al., 2006), from the T1-weighted scans. Each participant's structural scan was then co-registered to the fMRI scan using rigid registration.

All analyses were done in the individual's native space rather than transforming all data to a common template, to prevent excessive error (Nieto-Castanon et al., 2003; Ozcan et al., 2005), particularly in small subcortical regions such as the basal ganglia, as we have specifically shown in individuals with Parkinson's disease (Chen et al., 2009; Ng et al., 2009). Nuisance regression was then used to remove several sources of variance such as head motion parameters, their temporal derivatives and their squares, white-matter signal, and the cerebrospinal fluid signal. The fMRI signal was then detrended and iteratively smoothed until it reached 6 full width at half maximum of smoothness. Finally, the fMRI signal was high-pass filtered using a 0.01 Hz filter cut-off. The preprocessed time courses of the voxels within each ROI were averaged as the overall activity of the ROI.

2.6. Effective brain connectivity analysis

Effective connectivity, which captures the causal and dynamic influence brain regions exert over one another and reveals the strength and directionality of information flow between brain regions (Appel-Cresswell et al., 2010; Friston, 2011), was computed between the 57 FreeSurfer-derived ROIs using the PCfdr (Peter Spirtes and Clark Glymour, false discovery rate) algorithm (Li et al., 2008a; Li and Wang, 2009). This algorithm is specifically designed to assess connectivity

when a relatively large number of ROIs and relatively few time points are available. It explores the dependence/independence between pairs of ROIs conditional on an exhaustive search of all other ROI combinations. The FDR threshold was set to 5%. We pooled the Parkinson's disease and control groups together and computed the significant connections amongst ROIs for all tasks. The strength and direction of significant connections between ROIs were determined using a dynamic Bayesian network (DBN) group analysis approach (Li et al., 2006, 2007, 2008b).

Four separate statistical models were created utilizing binomial logistic regression: contrasting SB vs {rest, proprioception} and DB vs {rest, proprioception} for both individuals with Parkinson's disease and control groups. Principal component analysis (PCA) was employed to achieve dimensionality reduction for the significant connections detected by the PCfdr/DBN method. PCA was performed separately for controls and individuals with Parkinson's disease. The first 12 principal components (PCs), explaining at least 75% of the variance in both groups, were selected. Overall model fits were determined by comparing the full model to an intercept only model using the log-likelihood test.

Only the DB vs {rest, proprioception} models for controls and individuals with Parkinson's disease were statistically significant (see RESULTS), and thus these models were investigated further. The β regression coefficients and their Wald χ^2 statistic were examined to determine which PCs were making a significant contribution to the prediction of the task. Connections with the largest effect on each significant PC were identified by converting the PCA loadings into Z-scores and selecting all connections with an absolute Z-score ≥ 1.96. To evaluate the ability of the logistic regression models to correctly predict the task category of observed cases, contingency tables and leave-one-out cross validation were used, followed by two-tailed Fisher's Exact Tests of independence to examine the relationship between performed and predicted tasks.

In order to directly compare relevant connections between controls and individuals with Parkinson's disease, we first took the union of the connections significant in the DB task in either individuals with Parkinson's disease or controls. We then performed logistic regression with Least Absolute Shrinkage and Selection Operator (LASSO) regularization to identify connections predicting group membership. An $\alpha < 0.05$ was used for all statistical comparisons.

2.7. Participant baseline characteristics and head motion parameters

For both participant baseline characteristics and head motion parameters, assumptions of normality were validated using Shapiro-Wilk's test and inspection of histograms and quantile–quantile plots. Baseline characteristics between controls and individuals with Parkinson's disease were compared using independent *t*-tests or Fisher's Exact Tests where appropriate. Mean volume-to-volume framewise displacements, used to assess head motion, were log-transformed due to non-normality and subsequently analyzed using a 2 × 4 mixed design ANOVA with group (Parkinson's disease, controls) and task (rest, proprioception, SB, DB) as independent variables. In the case where Mauchly's tests of sphericity ($p < 0.05$) was significant, the Greenhouse-Geisser ε statistic was used. An $\alpha < 0.05$ was used for all statistical comparisons. In case of significant main and interaction effects, post hoc comparisons were performed after adjusting for multiple comparisons using a Bonferroni correction.

2.8. Data availability

De-identified data are available from the corresponding author upon reasonable request.

3. Results

3.1. Head motion

Minimal head motion occurred during the MRI scans; for both groups mean volume-to-volume framewise displacement was <0.3 mm in all tasks (Table 3). This is comparable to head motion reported previously during resting-state fMRI in older adults (Li et al., 2017) and fMRI during a foot-pedalling task in individuals with Parkinson's disease (Matar et al., 2019). No significant main effects of task or group, or interaction effects, were found for mean framewise displacement.

3.2. Effective connectivity

The PCfdr/DBN method detected 164 significant connections between ROIs, which represent ~5.1% of all possible (57 × 56 = 3,192) directional connections. PCA of these 164 significant connections showed that the first 12 PCs contained 76% and 90% of the total variability for controls and individuals with Parkinson's disease respectively.

3.2.1. Static balancing task

In both controls and individuals with Parkinson's disease, the full model with 12 predictors was not significantly better at predicting the tasks compared to the constant only model (controls: $\chi^2[12, N = 51] = 18.632$, $p = 0.098$; individuals with Parkinson's disease: $\chi^2[12, N = 51] = 10.706$, $p = 0.554$).

3.2.1.1. Dynamic balancing task. In controls, the log-likelihood test indicated that the full model with 12 predictors was significantly better at predicting the tasks compared to the constant only model ($\chi^2[12, N = 51] = 43.286$, $p = 2e^{-5}$). The full model was able to correctly classify 97% of the resting/proprioceptive tasks and 94% of the DB tasks, for an overall success rate of 96%. Fisher's Exact Test indicated there was a statistically significant relationship between the performed and predicted tasks ($p < 0.0001$, odds ratio [95% asymptotic confidence interval] = 528.000 [30.991, 8995.500]). During leave-one-out cross validation, the full model was able to correctly classify 88% of the resting/proprioceptive tasks and 47% of the DB tasks, for an overall success rate of 75%. There was a statistically significant relationship between the performed and predicted tasks ($p = 0.012$, 6.667 [1.623, 27.377]). Examination of the β coefficients and their Wald χ^2 statistic showed 4 PCs making a significant contribution to the prediction of the DB task (Table 4). In general, the connections with the largest effect on the significantly contributing PCs connect the following areas (number of corresponding connections in brackets): brainstem to either cerebellum (2), limbic (1), thalamus (1), or other brainstem structures (1); limbic to other limbic (2) or basal ganglia structures (2); motor to other motor areas (4); frontal to other frontal (2) or basal ganglia structures (1); temporal to frontal (4) or limbic areas (3); and parietal to frontal (1) or temporal areas (1) (Table 5, Fig. 2A and 2B).

In individuals with Parkinson's disease, the log-likelihood test showed that the full model was significantly better at predicting the outcomes compared to the constant only model ($\chi^2[12, N = 51] = 46.982$, $p = 5e^{-6}$). The full model correctly classified 97% of the resting/proprioceptive tasks and 88% of the DB tasks, for an overall success rate

Table 3
Mean volume-to-volume framewise displacement.

Task	Parkinson	Control
Rest	0.16 (0.01)	0.19 (0.02)
Proprioception	0.26 (0.05)	0.17 (0.02)
Static balancing	0.16 (0.02)	0.17 (0.02)
Dynamic balancing	0.27 (0.03)	0.23 (0.02)

Data are displayed as mean (SE)

Table 4
Multiple binomial logistic regression models.

Predictor	β	SE β	Wald's χ^2	df	p	OR
Elderly controls - DB task (H-DB)						
Constant	−3.023	1.259	5.765	1	0.016	0.049
H-DB PC-1	0.236	0.277	0.723	1	0.395	1.266
H-DB PC-2	0.457	0.531	0.740	1	0.390	1.579
H-DB PC-3	0.814	0.565	2.078	1	0.149	2.258
H-DB PC-4	−0.078	0.622	0.016	1	0.901	0.925
H-DB PC-5	−0.452	0.709	0.405	1	0.524	0.637
H-DB PC-6	1.954	1.061	3.390	1	0.066	7.058
H-DB PC-7	**2.600**	**1.077**	**5.829**	**1**	**0.016**	**13.462**
H-DB PC-8	2.046	1.383	2.189	1	0.139	7.735
H-DB PC-9	**−6.384**	**2.719**	**5.512**	**1**	**0.019**	**0.002**
H-DB PC-10	0.047	0.952	0.002	1	0.961	1.048
H-DB PC-11	**−6.428**	**2.646**	**5.902**	**1**	**0.015**	**0.002**
H-DB PC-12	**−4.827**	**2.288**	**4.450**	**1**	**0.035**	**0.008**
Individuals with Parkinson's disease - DB task (P-DB)						
Constant	−3.363	1.047	10.327	1	0.001	0.035
P-DB PC-1	**−1.300**	**0.549**	**5.610**	**1**	**0.018**	**0.272**
P-DB PC-2	**−1.545**	**0.504**	**9.383**	**1**	**0.002**	**0.213**
P-DB PC-3	**1.061**	**0.446**	**5.658**	**1**	**0.017**	**2.890**
P-DB PC-4	−0.236	0.293	0.650	1	0.420	0.790
P-DB PC-5	0.185	0.494	0.141	1	0.708	1.203
P-DB PC-6	1.514	0.860	3.097	1	0.078	4.545
P-DB PC-7	0.991	1.090	0.826	1	0.364	2.693
P-DB PC-8	**8.977**	**2.834**	**10.031**	**1**	**0.002**	**7917.000**
P-DB PC-9	0.802	1.528	0.275	1	0.600	2.230
P-DB PC-10	0.670	1.019	0.431	1	0.511	1.953
P-DB PC-11	**−2.996**	**1.524**	**3.866**	**1**	**0.049**	**0.050**
P-DB PC-12	−2.750	1.448	3.606	1	0.058	0.064

β = beta coefficient, SE β = standard error of beta coefficient, Wald's χ^2 = Wald's chi-square statistic, df = degrees of freedom, p = significance Wald's χ^2, OR = odds ratio (equal to exp(β)). Bolded predictors made a significant contribution to the prediction of the task.

of 94%. Fisher's Exact Test indicated there was a statistically significant relationship between the performed and predicted tasks ($p < 1e^{-4}$, 247.500 [20.792, 2946.100]). During leave-one-out cross validation, the full model was able to correctly classify 88% of the resting/proprioceptive tasks and 71% of the DB tasks, for an overall success rate of 82%. There was a statistically significant relationship between the performed and predicted tasks ($p = 4e^{-5}$, 18.000 [4.116, 78.711]). Examination of the β coefficients and their Wald χ^2 statistic showed 5 PCs making a significant contribution to the prediction of the DB task (Table 4). In general, the connections with the largest effect on the significantly contributing PCs connect the following areas (number of corresponding connections in brackets): brainstem to either cerebellum (2), limbic (2), thalamus (1), or basal ganglia structures (2); limbic to other limbic (2) or basal ganglia structures (1); motor to other motor (2) or frontal areas (1); frontal to other frontal (2) or basal ganglia structures (1); temporal to either frontal (2), limbic (2), or other temporal areas (1); and parietal to other parietal areas (1) (Table 6, Fig. 3A and 3B).

To directly compare between groups, 34 connections, making a significant contribution to predicting the DB task in controls and/or individuals with Parkinson's disease, were entered in the logistic LASSO regression. Five connections survived, indicating that they are important to predicting group membership (control or individual with Parkinson's disease) during the DB task (Table 7). The connections predicting group membership involve the following areas: midbrain to left nucleus accumbens, left anterior cingulate cortex to left caudate, right insular cortex to left insular cortex, left dorsal premotor area to left pre-supplementary motor area, and right middle temporal cortex to right lateral orbitofrontal cortex.

4. Discussion

We used a novel MRI-compatible balance simulator (Pasman et al., 2019) to investigate effective brain connectivity patterns related to static and dynamic balance-related tasks in individuals with Parkinson's disease and healthy older adults. The simulator provides a unique opportunity to study brain activation in participants during balance-like movements in the MRI scanner, as it requires the static and dynamic reactive control of an unstable inverted pendulum system through the activation of anti-gravity muscles around the ankle joint. This ensures that both motor and proprioceptive sensory pathways are engaged during the task in a way that is similar to upright standing, unlike prior studies that relied on motor imagery of balance. We showed that a network of cortical and subcortical neural structures, including frontal, parietal, and temporal cortices as well as basal ganglia, cerebellum, and brainstem, was active during dynamic balancing in healthy older adults. In individuals with Parkinson's disease, a similar network of cortical and subcortical neural structures was active during dynamic balancing, however, the strength and direction of connections between certain areas were different.

4.1. Effective connectivity network for dynamic balancing in healthy older adults

We observed decreased connectivity between different motor areas and increased connectivity from the brainstem to several cortical and subcortical areas in healthy older adults during dynamic balancing compared to the rest/proprioception conditions. Taken together, this indicates a preference of subcortical over motor cortical control of dynamic balancing in healthy older adults. Our results are generally consistent with prior results from motor imagery studies that identified several subcortical (e.g., mesencephalic locomotor region, thalamus, cerebellum, and basal ganglia) and cortical (e.g., frontal, temporal, parietal, and cingulate cortices) areas as part of a distributed dynamic balance network (Ferraye et al., 2014; Taube et al., 2015; Bhatt et al., 2018; Mouthon et al., 2018). Additionally, our results provide novel insight into the directionality of the connections between these areas and highlighting the potential context- and task-specificity of supplementary motor area (SMA) activity during dynamic balance tasks.

4.1.1. Connectivity involving subcortical and brainstem regions increases in healthy older adults during dynamic balancing

As shown in Fig. 2B, connectivity increased from the dorsolateral prefrontal and anterior cingulate cortices to the basal ganglia, more specifically the caudate nucleus, in healthy elderly during dynamic balancing. This finding is consistent with fMRI evidence of increased activation in the prefrontal and anterior cingulate cortices, as well as in the basal ganglia (putamen and globus pallidus), during motor imagery of dynamic balance tasks (Ferraye et al., 2014; Taube et al., 2015; Bhatt et al., 2018; Mouthon et al., 2018). Increased activity in prefrontal and anterior cingulate cortices during dynamic balance responses has also been implicated with EEG and fNIRS (Mihara et al., 2008; Sipp et al., 2013; Bogost et al., 2016; Solis-Escalante et al., 2019).

The involvement of the prefrontal cortex during dynamic balancing that we observed is consistent with its role in error detection (Bogost et al., 2016) and monitoring postural stability (Solis-Escalante et al., 2019) through sensory integration and allocation of attentional resources (Mihara et al., 2008; Teo et al., 2018). The anterior cingulate also plays an important role in monitoring motor error which is critical for detecting loss of balance during challenging posture and gait tasks (Sipp et al., 2013; Marlin et al., 2014; Bhatt et al., 2018; Goel et al., 2019). The basal ganglia have long been linked to balance control, particularly in terms of sensorimotor integration, gain control of balance correcting responses, and proper selection and execution of context-specific balance correcting responses (Visser and Bloem, 2005; Jacobs and Horak, 2007; Ferraye et al., 2014; Taube et al., 2015). Therefore, the observed increase in connectivity from the prefrontal and anterior cingulate cortices to the basal ganglia during our simulated dynamic balance task adds further evidence for the critical role of these areas in maintaining balance control.

We also found increased connectivity from pons to cerebellum, and

Table 5
Connections with largest effect on the significant principal components predicting dynamic balance task in controls.

PC	Connection from	Connection to	From area	To area	Loading	Z-score	Strength RL/PL	Strength DL	Δ Strength	Direction
PC-7										
	Pons	L cerebellum	BS	CER	0.455	5.810	0.376	0.453	−0.077	↑
	R superior frontal ctx	R dorsolateral prefrontal ctx	FRON	FRON	0.191	2.448	0.286	0.543	−0.257	↑
	Midbrain	L insular ctx	BS	LIMB	−0.206	−2.630	0.607	0.993	−0.386	↑
	Midbrain	L thalamus	BS	THAL	−0.246	−3.141	0.531	0.780	−0.249	↑
	L superior temporal ctx	L amygdala	TEMP	LIMB	−0.257	−3.282	0.392	0.398	−0.006	↑
	L middle temporal ctx	L amygdala	TEMP	LIMB	0.397	5.078	0.346	0.335	0.010	↓
	Midbrain	L cerebellum	BS	CER	−0.181	−2.310	0.358	0.265	0.093	↓
	R pre-SMA	L pre-SMA	MOT	MOT	−0.184	−2.347	0.584	0.469	0.115	↓
PC-9										
	Pons	L cerebellum	BS	CER	0.400	5.170	0.376	0.453	−0.077	↑
	R anterior cingulate ctx	R caudate	LIMB	BG	−0.165	−2.059	0.201	0.489	−0.288	↑
	R inferior temporal ctx	R lateral orbitofrontal ctx	TEMP	FRON	−0.189	−2.363	0.178	0.297	−0.119	↑
	R middle temporal ctx	R lateral orbitofrontal ctx	TEMP	FRON	0.352	4.549	0.393	0.375	0.019	↓
	R dorsal premotor area	R SMA	MOT	MOT	0.168	2.204	0.393	0.295	0.098	↓
	L inferior parietal ctx	L middle temporal ctx	PAR	TEMP	0.166	2.171	0.310	0.264	0.046	↓
	L inferior parietal ctx	L dorsolateral prefrontal ctx	PAR	FRON	0.163	2.130	0.247	0.222	0.025	↓
	Midbrain	L cerebellum	BS	CER	−0.238	−2.997	0.358	0.265	0.093	↓
PC-11										
	R superior temporal ctx	L amygdala	TEMP	LIMB	0.300	3.794	0.317	0.384	−0.067	↑
	R lateral orbitofrontal ctx	R medial orbitofrontal ctx	FRON	FRON	0.242	3.054	0.530	0.574	−0.045	↑
	L middle temporal ctx	L lateral orbitofrontal ctx	TEMP	FRON	−0.163	−2.121	0.201	0.310	−0.109	↑
	R amygdala	L amygdala	LIMB	LIMB	−0.163	−2.124	0.457	0.478	−0.021	↑
	L anterior cingulate ctx	L caudate	LIMB	BG	−0.208	−2.693	0.168	0.304	−0.135	↑
	R anterior cingulate ctx	R caudate	LIMB	BG	−0.221	−2.862	0.201	0.489	−0.288	↑
	L SMA	L pre-SMA	MOT	MOT	−0.226	−2.921	0.209	0.391	−0.182	↑
	L dorsal premotor area	L pre-SMA	MOT	MOT	0.305	3.855	0.445	0.441	0.005	↓
	Pons	Midbrain	BS	BS	0.211	2.655	0.302	0.206	0.096	↓
	L middle temporal ctx	L amygdala	TEMP	LIMB	−0.240	−3.109	0.346	0.335	0.010	↓
	Midbrain	L cerebellum	BS	CER	−0.261	−3.379	0.358	0.265	0.093	↓
PC-12										
	R lateral orbitofrontal ctx	R medial orbitofrontal ctx	FRON	FRON	0.247	3.073	0.530	0.574	−0.045	↑
	R superior temporal ctx	L amygdala	TEMP	LIMB	0.212	2.625	0.317	0.384	−0.067	↑
	R insular ctx	L insular ctx	LIMB	LIMB	0.172	2.113	0.546	0.572	−0.027	↑
	R middle temporal ctx	R medial orbitofrontal ctx	TEMP	FRON	−0.147	−1.981	0.200	0.307	−0.107	↑
	Pons	L cerebellum	BS	CER	−0.160	−2.149	0.376	0.453	−0.077	↑
	R inferior temporal ctx	R lateral orbitofrontal ctx	TEMP	FRON	−0.193	−2.571	0.178	0.297	−0.119	↑
	R dorsolateral prefrontal ctx	R caudate	FRON	BG	−0.196	−2.614	0.353	0.357	−0.004	↑
	L superior temporal ctx	L amygdala	TEMP	LIMB	−0.245	−3.233	0.392	0.398	−0.006	↑
	Midbrain	L cerebellum	BS	CER	0.333	4.176	0.358	0.265	0.093	↓
	R middle temporal ctx	R lateral orbitofrontal ctx	TEMP	FRON	0.268	3.347	0.393	0.375	0.019	↓
	R dorsal premotor area	R SMA	MOT	MOT	0.214	2.650	0.393	0.295	0.098	↓
	L inferior parietal ctx	L middle temporal ctx	PAR	TEMP	−0.151	−2.036	0.310	0.264	0.046	↓

PC = principal component, R = right, L = left, ctx = cortex, SMA = supplementary motor area, BS = brainstem, CER = cerebellum, TEMP = temporal, LIMB = limbic, FRON = frontal, MOT = motor, THAL = thalamus, PAR = parietal

midbrain to thalamus and insular cortex (Fig. 2B). These results are consistent with prior findings from motor imagery of dynamic balance tasks that have demonstrated increased activation of the pons and mesencephalic locomotor region of the midbrain (Ferraye et al., 2014), and increased activation of the cerebellum, thalamus, and insula (Ferraye et al., 2014; Taube et al., 2015; Bhatt et al., 2018). Increased connectivity between brainstem structures, the thalamus, and cerebellum supports growing evidence for the importance of the corticopontocerebellar-thalamocortical loop in integrating feedforward commands with sensory information to shape and modulate subsequent motor commands (MacKinnon, 2018) and allows for postural responses to be modified by prior experience and changes in central set (Jacobs & Horak, 2007; Bhatt et al., 2018).

Several areas in the pons are thought to be involved in balance control, including the pontomedullary reticular formation, locus coeruleus, and vestibular nuclei (Takakusaki, 2017; MacKinnon, 2018). The vestibular nuclei contribute to the modulation of dynamic balance responses through descending vestibular-spinal pathways, ascending projections to the thalamus and insula, and bidirectional connections to the vermis and flocculonodular nuclei of the cerebellum (Takakusaki, 2017; MacKinnon, 2018). The increased connectivity observed during dynamic balancing from pons to cerebellum, supports extensive evidence for the vestibulo-cerebellar networks crucial role in maintaining postural control (Carpenter et al., 2001; Morton & Bastian, 2004; Schniepp et al., 2017), allowing for efferent and afferent proprioceptive and vestibular inputs to be compared in order to rapidly identify and correct movement error associated with a balance disturbance (Peterka, 2018). Nuclei within the midbrain have also been linked to postural control, including the mesencephalic locomotor region (composed of the cuneiform nucleus and pedunculopontine nucleus) and caudal raphe nuclei (Takakusaki, 2017; MacKinnon, 2018). The pedunculopontine nucleus has connections with the basal ganglia and limbic areas, thalamus, cerebellum, brainstem, spinal cord, and cerebral cortex (Alam et al., 2011). The observed connection from midbrain to thalamus makes sense given the role of the posterolateral thalamus in maintaining upright posture (Masdeu and Gorelick, 1988), and verticality perception (Jacobs & Horak, 2007; Barra et al., 2010). The parieto-insular vestibular cortex, which includes part of the posterior insula and parietal operculum, as well as part of the temporo-perisylvian cortex in the superior temporal gyrus, has strong connections with other vestibular-related cortical areas, and receives converging sensory inputs (Indovina et al., 2015; Takakusaki, 2017). This region is thought to be essential for sensory integration during postural tasks (Jacobs & Horak, 2007), contributing to perception of visual and perceived gravitational vertical (Jacobs & Horak, 2007; Takakusaki, 2017) and spatial orientation and self-motion perception (Taube et al., 2015; Bhatt et al., 2018).

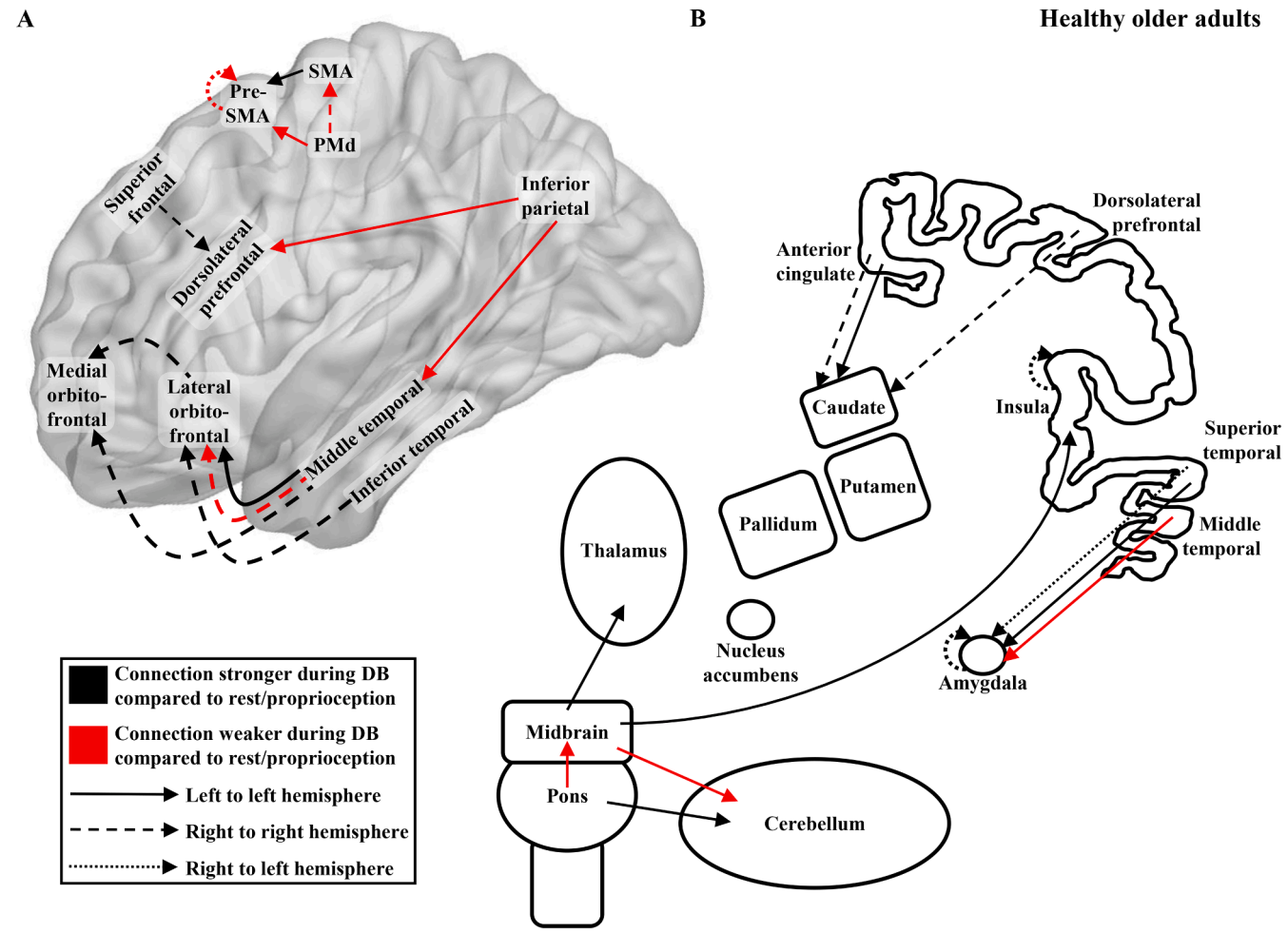

Fig. 2. Effective connectivity network found in healthy older adults during the dynamic balancing task.

Healthy older adults also showed increased connectivity from temporal cortices to both subcortical and other cortical areas (Fig. 2A and 2B). Connectivity increased from the superior temporal cortex to the amygdala, as well as middle temporal cortex and inferior temporal cortex to the lateral and medial orbitofrontal cortices. The superior temporal gyrus was found to be activated in previous studies during motor imagery of dynamic balancing (Taube et al., 2015), and its temporo-perisylvian cortex is part of the parieto-insular vestibular cortex (Indovina et al., 2015).

4.1.2. Connectivity involving motor and parietal regions decreases in healthy older adults during dynamic balancing

Our results indicate that healthy older adults, when performing simulated dynamic balance, had decreased connectivity from the dorsal premotor area to SMA and pre-SMA, as well as the right to left pre-SMA (Fig. 2A). Our observation of reduced connectivity between and within motor cortical areas is in contrast to prior evidence of increased premotor and SMA activity recorded with MRI during motor imagery of dynamic balance tasks (Ferraye et al., 2014; Taube et al., 2015; Bhatt et al., 2018; Mouthon et al., 2018). This discrepancy between the current study and prior motor imagery studies could be due to differences in the level of automaticity associated with the dynamic balance tasks. The dynamic balance task used in the current study resembles an externally triggered movement, that required rapid ankle responses to transient, unpredictable perturbations in random directions, that have components considered to be more automatic and reflexive (Carpenter et al., 2001). Reduced activation of pre-SMA, premotor areas, and superior and inferior parietal areas has been reported in healthy older adults as tasks become more automatic (Wu and Hallett, 2005a). In contrast to the dynamic balance-simulator task used in the current study, Ferraye et al. (2014) used a voluntary sway task which requires feedforward coordination of postural adjustments to the voluntary sway movements. In addition, internally and externally triggered movements are associated with different brain activation patterns, with increased activation in SMA during internally driven compared to externally triggered movements (Filyushkina et al., 2019). The SMA and premotor areas are most critical in preparing planned or complex motor programs (Takakusaki, 2017; MacKinnon, 2018) and thus more likely to contribute to balance tasks that require more feedforward, less automatic balance control (Ferraye et al., 2014; Mierau et al., 2015; Takakura et al., 2015), and/or later phases of the compensatory balance reactions such as stepping or reaching responses (Mihara et al., 2008; Marlin et al., 2014).

4.2. Dynamic balancing relies more on cortical than subcortical control in individuals with Parkinson's disease

When individuals with Parkinson's disease were asked to perform a dynamic balancing task, compared to the rest/proprioception tasks, they showed an effective connectivity pattern largely similar to healthy older adults. However, there were some notable differences. Individuals with Parkinson's disease had increased connectivity associated with motor control and parietal areas, and decreased connectivity from brainstem to other subcortical areas, suggesting that dynamic balance control in individuals with Parkinson's disease relies relatively more on cortical motor areas. The increased cortical involvement we observed in individuals with Parkinson's disease during dynamic balancing compared

Table 6
Connections with largest effect on the significant principal components predicting dynamic balance task in individuals with Parkinson's disease.

PC	Connection from	Connection to	From area	Toarea	Loading	Z-score	Strength RL/PL	Strength DL	Δ Strength	Direction
PC-1										
	Midbrain	L amygdala	BS	LIMB	0.987	12.566	2.600	1.133	1.467	↓
PC-2										
	Midbrain	R pallidum	BS	BG	−0.173	−2.269	1.147	2.194	−1.047	↑
	Midbrain	L nucleus accumbens	BS	BG	0.947	12.051	1.716	0.960	0.757	↓
PC-3										
	Midbrain	R pallidum	BS	BG	0.923	11.764	1.147	2.194	−1.047	↑
	Pons	R insular ctx	BS	LIMB	0.222	2.725	0.969	1.206	−0.237	↑
	Midbrain	L nucleus accumbens	BS	BG	0.181	2.189	1.716	0.960	0.757	↓
PC-8										
	L superior temporal ctx	L amygdala	TEMP	LIMB	0.299	3.722	0.371	0.486	−0.115	↑
	R lateral orbitofrontal ctx	R medial orbitofrontal ctx	FRON	FRON	0.231	2.851	0.507	0.578	−0.071	↑
	R middle temporal ctx	R lateral orbitofrontal ctx	TEMP	FRON	0.176	2.134	0.273	0.498	−0.225	↑
	R anterior cingulate ctx	L anterior cingulate ctx	LIMB	LIMB	0.172	2.088	0.578	0.790	−0.212	↑
	R superior frontal ctx	R dorsolateral prefrontal ctx	FRON	FRON	0.165	1.996	0.379	0.476	−0.097	↑
	L middle temporal ctx	L amygdala	TEMP	LIMB	−0.259	−3.464	0.314	0.400	−0.086	↑
	R middle temporal ctx	R medial orbitofrontal ctx	TEMP	FRON	−0.259	−3.464	0.308	0.346	−0.038	↑
	Midbrain	L cerebellum	BS	CER	0.197	2.404	0.465	0.426	0.039	↓
	Midbrain	L thalamus	BS	THAL	0.190	2.323	0.786	0.677	0.109	↓
	R dorsal premotor area	R dorsolateral prefrontal ctx	MOT	FRON	−0.170	−2.319	0.373	0.310	0.064	↓
	R insular ctx	R amygdala	LIMB	LIMB	−0.179	−2.432	0.688	0.584	0.105	↓
PC-11										
	Pons	L cerebellum	BS	CER	0.287	3.716	0.399	0.722	−0.323	↑
	L dorsal premotor area	L pre-SMA	MOT	MOT	0.175	2.282	0.449	0.788	−0.339	↑
	R superior parietal ctx	R precuneus	PAR	PAR	0.161	2.096	0.216	0.250	−0.033	↑
	R middle temporal ctx	L middle temporal ctx	TEMP	TEMP	−0.170	−2.123	0.340	0.384	−0.043	↑
	R anterior cingulate ctx	R caudate	LIMB	BG	−0.198	−2.489	0.183	0.410	−0.226	↑
	L SMA	L pre-SMA	MOT	MOT	−0.213	−2.676	0.239	0.304	−0.065	↑
	Midbrain	L cerebellum	BS	CER	0.434	5.593	0.465	0.426	0.039	↓
	R dorsolateral prefrontal ctx	R caudate	FRON	BG	0.213	2.771	0.311	0.245	0.066	↓
	R insular ctx	R amygdala	LIMB	LIMB	0.176	2.287	0.688	0.584	0.105	↓
	Midbrain	L thalamus	BS	THAL	0.157	2.050	0.786	0.677	0.109	↓

PC = principal component, R = right, L = left, ctx = cortex, SMA = supplementary motor area, BS = brainstem, BG = basal ganglia, CER = cerebellum, TEMP = temporal, LIMB = limbic, FRON = frontal, MOT = motor, THAL = thalamus, PAR = parietal

to healthy older adults is consistent with the 'posture second strategy' observed in individuals with Parkinson's disease, whereby engagement in a mental task (e.g., mental arithmetic) results in disproportionate decreases in postural control (Bloem et al., 2006).

4.2.1. *Cortical connectivity was generally increased in individuals with Parkinson's disease during dynamic balancing*

In contrast to healthy older adults who showed decreased connectivity associated with motor control areas and the inferior parietal cortex (Fig. 2A), individuals with Parkinson's disease had increased connectivity from the SMA and premotor areas to the pre-SMA, and from the superior parietal cortex to precuneus (Fig. 3A). Increased activation in the pre-SMA and SMA was previously found in individuals with Parkinson's disease 'on' medication, compared to healthy older adults, during active, but not passive, ankle movements (Katschnig et al., 2011). Our findings are also in line with previous observations of reduced activation in motor control and parietal areas in healthy older adults (Wu and Hallett, 2005a), but increased activation in the cerebellum, motor, parietal, and prefrontal areas in individuals with Parkinson's disease 'off' medication (Wu and Hallett, 2005b), during automatic movements. Therefore, it seems as if individuals with Parkinson's disease 'off' medication compensate for their inefficient brain activity with increased premotor-parietal region activation during execution of automatic movements (Wu and Hallett, 2005b). The qualitative differences in connectivity associated with motor control areas were supported with direct statistical comparison between the groups. In particular, individuals with Parkinson's disease were best discriminated from the healthy older adults by an abnormal increase in connectivity from the dorsal premotor area to the pre-SMA.

While cortical connectivity increased in motor and parietal areas, connectivity from the dorsal prefrontal and anterior cingulate cortices to the caudate nucleus were reduced in individuals with Parkinson's disease compared to healthy older adults. Reduced activity in the superior parietal and anterior cingulate cortices was found previously during motor imagery of gait in individuals with Parkinson's disease 'off' medication compared to healthy older adults (Snijders et al., 2011). Direct statistical comparison between the groups confirmed that a lack of normal increase in connectivity strength from the anterior cingulate cortex to the caudate nucleus was important in discriminating individuals with Parkinson's disease from healthy older adults. In addition, an abnormal increase in connectivity from the middle temporal cortex to lateral orbitofrontal cortex, and lack of normal increase between the bilateral insular cortices were also important in best discriminating individuals with Parkinson's disease from health older adults during dynamic balancing.

4.2.2. *Subcortical connectivity was altered in individuals with Parkinson's disease during dynamic balancing.*

Reduced connectivity was seen in individuals with Parkinson's disease from the midbrain to thalamus, cerebellum, nucleus accumbens, and amygdala (Fig. 3B). These findings corroborate previous work which found that the tendency to shift execution of automatic movements to subcortical areas is less clear in individuals with Parkinson's disease 'off' medication compared to healthy older adults (Wu et al., 2010). Some of the subcortical connections identified in predicting the dynamic balancing task in individuals with Parkinson's disease, such as the connections from the midbrain to thalamus and cerebellum, were common to both groups. However, unique connections in individuals with Parkinson's disease included reduced connectivity from midbrain to nucleus accumbens and amygdala, and increased connectivity from midbrain to the pallidum and pons to insular cortex. Direct statistical comparison between the groups confirmed an abnormal decrease in connectivity from the midbrain to nucleus accumbens was important in discriminating individuals with Parkinson's disease from health older

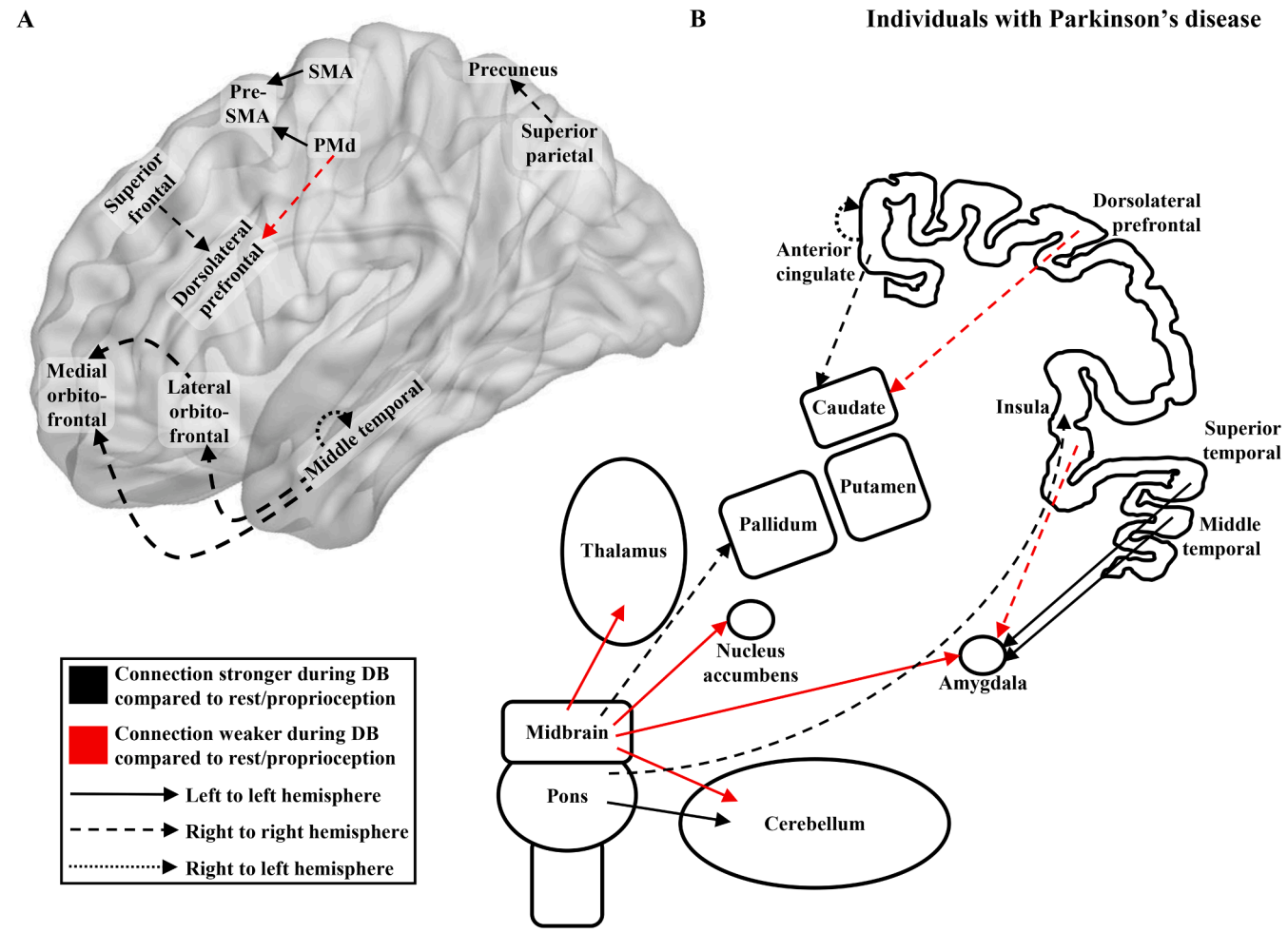

Fig. 3. Effective connectivity network found in individuals with Parkinson's disease during the dynamic balancing task.

Table 7
Multiple binomial logistic LASSO regression model predicting group membership in the dynamic balance task.

	Predictor	Connection from	Connection to	From	To	β
DB	Constant					−0483
	Conn-1	L dorsal premotor area	L pre-SMA	MOT	MOT	1.246
	Conn-2	R middle temporal ctx	R lateral orbitofrontal ctx	TEMP	FRON	0.618
	Conn-3	Midbrain	L nucleus accumbens	BS	BG	−0.067
	Conn-4	L anterior cingulate ctx	L caudate	LIMB	BG	−0.629
	Conn-5	R insular ctx	L insular ctx	LIMB	LIMB	−0.640

DB = dynamic balance, R = right, L = left, ctx = cortex, SMA = supplementary motor area, BS = brainstem, BG = basal ganglia, TEMP = temporal, LIMB = limbic, MOT = motor, β = beta coefficient.

adults.

4.3. Effective connectivity network for static balancing

In both healthy older adults and individuals with Parkinson's disease we were unable to determine an effective connectivity network associated with the static balance task, compared to rest and proprioception tasks. Our results suggest that the brain connectivity network associated with the simulated static balancing task might not have been distinct enough from that associated with the proprioception task, involves a more distributed network, or may be controlled using predominantly passive stiffness and spinal reflex mechanisms (Winter et al., 1998). Our current protocol prioritized proprioceptive feedback, since the task was performed with the eyes closed, and no head rotational or translational inputs would be detected by vestibular receptors due to participants lying supine with the head fixed. However, this does not suggest that the vestibular system is inactive during our simulated balance task, since otoliths would still be activated by gravity, and the vestibular nuclei also integrate non-labyrinthine inputs from cortical, subcortical, and spinal cord pathways, including proprioceptive inputs from the limbs (McCall et al., 2017). Although congruent sensory information is normally available from multiple sensory systems during upright stance, the simulated static balance task used in the current study is still relevant, since balance can also be maintained by the central nervous system even in the absence of reliable vestibular and visual inputs. This is due to redundancy and the ability of the central nervous system to re-weigh sensory information (Peterka, 2018). Furthermore, similar balance deficits with Parkinson's disease have been observed during real and simulated static and dynamic balance tasks with and without vision (Pasman et al., 2019). Future studies could introduce more balance-relevant sensory inputs by incorporating real-time visual feedback (Pasman et al., 2019) or electrical vestibular stimulation to determine whether additional sources of sensory information provide more distinct connectivity models for static balance control.

4.4. Limitations and future directions

For both the static and dynamic balancing tasks, the connectivity of cortical regions involved in sensory integration, such as parietal areas, could have been affected by the limited availability of balance-relevant sensory information, other than proprioceptive feedback. Future studies should investigate how the addition of visual information (i.e., real-time visual feedback from a virtual reality scene driven by the output from a potentiometer attached to the axis of the simulator) and/or vestibular information (i.e., using electrical vestibular information) changes the connectivity of these particular regions during the simulated balance tasks.

While all participants were familiarized with the balance simulator in a session separate from the MRI scanning session, differences between individuals with Parkinson's disease and healthy older adults regarding motor learning and retention may have contributed to the difference in cortical and subcortical control between the groups during the novel simulated balance task (Marinelli et al., 2017).

The conscious nature of the proprioceptive (i.e., finger tracking) task used as the control task may have resulted in a downplay of the role of cortical cognitive centers during the simulated balance tasks.

Using the simulator in its current form, it is not possible to assess medial–lateral balance control. However, while different muscle/joints are involved in controlling anterior-posterior and medial–lateral postural sway, there is no evidence to suggest they are controlled using different cortical or subcortical structures.

The risk of head movements was increased due to the clinical population investigated and the tasks with lower leg motion used. During data collection, head motion was minimized by immobilizing the participant's head using straps and foam, as well as stabilizing participant's hips using weights (see METHODS). Head motion, as assessed by mean volume-to-volume framewise displacement, was comparable to head motion reported previously (Li et al., 2017; Matar et al., 2019).

The individuals with Parkinson's disease included in this study consisted mostly of individuals with moderate disease (Table 2). Future work is needed to investigate whether the neural substrates associated with postural instability in individuals with Parkinson's disease change with disease severity. In addition, included individuals with Parkinson's disease also had relatively good cognition, which was required to comply with the task requirements. However, cognitive decline contributes to balance deficits in individuals with Parkinson's disease, and excluding cognitively impaired individuals – as we and many others have done (Domingos et al., 2015) – may create an incorrect perspective of the severest balance deficits in Parkinson's disease.

Future work is needed to correlate the neural substrates of balance control with the balance behaviour exhibited by participants when maintaining balance using the simulator or during upright standing. This provides the opportunity to investigate whether the neural substrates associated with postural instability in individuals with Parkinson's disease change with the severity of their balance deficits as measured using either clinical balance or posturographic measures.

All individuals with Parkinson's disease were tested during their subjectively best clinical 'on' condition as postural instability is often unaltered by dopaminergic medication (Grimbergen et al., 2009) and testing individuals with Parkinson's disease 'on' medication avoids any potential confounds of fatigue, anxiety, and cumbersome bradykinesia/rigidity that may accompany the 'off' phase. Future work is needed to investigate the effect of dopaminergic medication on the brain connectivity patterns associated with balance control by testing individuals with Parkinson's disease during both the 'on' and 'off' condition, as previous studies have shown levodopa reduces the utilization of motor reserve for compensation in individuals with Parkinson's disease (Palmer et al., 2009)

5. Conclusion

In conclusion, the results of this study indicate that a network of cortical and subcortical neural structures, including frontal, parietal, and temporal cortices as well as basal ganglia, thalamus, cerebellum, and brainstem, was active during dynamic balancing in healthy older adults. In individuals with Parkinson's disease a similar network of cortical and subcortical neural structures was found. However, dynamic balancing was more reliant on motor cortical control in individuals with Parkinson's disease compared to healthy older adults. The increased understanding of the neural substrates contributing to postural instability in Parkinson's disease provided by the novel MRI-compatible balance simulator could lead to new targets for improved pharmacological and neurosurgical interventions.

CRediT authorship contribution statement

Elizabeth P. Pasman: Conceptualization, Project administration, Formal analysis, Investigation, Methodology, Visualization, Writing - original draft. **Martin J. McKeown:** Conceptualization, Project administration, Methodology, Resources, Writing - review & editing. **Saurabh Garg:** Software, Data curation, Formal analysis, Writing - review & editing. **Taylor W. Cleworth:** Investigation, Formal analysis, Writing - review & editing. **Bastiaan R. Bloem:** Conceptualization, Writing - review & editing. **J. Timothy Inglis:** Conceptualization, Writing - review & editing. **Mark G. Carpenter:** Conceptualization, Resources, Methodology, Investigation, Writing - review & editing, Funding acquisition, Supervision.

Declaration of Competing Interest

The authors declare that they have no known competing financial interests or personal relationships that could have appeared to influence the work reported in this paper.

Acknowledgements

This work was funded by grants from Parkinson Canada and NSERC (MGC), and partly supported by the John Nichol Chair in Parkinson's Research (MJM).

Funding

Parkinson Canada (#2014-726); Natural Sciences and Engineering Research Council (NSERC) of Canada (#326910).

References

Alam, M., Schwabe, K., Krauss, J.K., 2011. The pedunculopontine nucleus area: critical evaluation of interspecies differences relevant for its use as a target for deep brain stimulation. Brain 134 (Pt 1), 11–23. https://doi.org/10.1093/brain/awq322.

Appel-Cresswell, S., de la Fuente-Fernandez, R., Galley, S., McKeown, M.J., 2010. Imaging of compensatory mechanisms in Parkinson's disease. [Review]. Curr. Opin. Neurol. 23 (4), 407–412. https://doi.org/10.1097/WCO.0b013e32833b6019.

Barra, J., Marquer, A., Joassin, R., Reymond, C., Metge, L., Chauvineau, V., et al., 2010. Humans use internal models to construct and update a sense of verticality. Brain 133 (Pt 12), 3552–3563. https://doi.org/10.1093/brain/awq311.

Bauer, C.E., Brefczynski-Lewis, J., Marano, G., Mandich, M.B., Stolin, A., Martone, P., et al., 2016. Concept of an upright wearable positron emission tomography imager in humans. Brain Behav. 6 (9) https://doi.org/10.1002/brb3.530.

Bhatt, T., Patel, P., Dusane, S., DelDonno, S.R., Langenecker, S.A., 2018. Neural Mechanisms Involved in Mental Imagery of Slip-Perturbation While Walking: A Preliminary fMRI Study. Front. Behav. Neurosci. 12, 203. https://doi.org/10.3389/fnbeh.2018.00203.

Billot, M., Simoneau, E.M., Van Hoecke, J., Martin, A., 2010. Age-related relative increases in electromyography activity and torque according to the maximal capacity during upright standing. Eur. J. Appl. Physiol. 109 (4), 669–680. https://doi.org/10.1007/s00421-010-1397-7.

Bloem, B.R., Grimbergen, Y.A., van Dijk, J.G., Munneke, M., 2006. The, "posture second" strategy: a review of wrong priorities in Parkinson's disease. [Review]. J. Neurol. Sci. 248 (1–2), 196–204. https://doi.org/10.1016/j.jns.2006.05.010.

Bogost, M.D., Burgos, P.I., Little, C.E., Woollacott, M.H., Dalton, B.H., 2016. Electrocortical Sources Related to Whole-Body Surface Translations during a Single- and Dual-Task Paradigm. Front. Hum. Neurosci. 10, 524. https://doi.org/10.3389/fnhum.2016.00524.

Boonstra, T.A., van der Kooij, H., Munneke, M., Bloem, B.R., 2008. Gait disorders and balance disturbances in Parkinson's disease: clinical update and pathophysiology. [Review]. Curr. Opin. Neurol. 21 (4), 461–471. https://doi.org/10.1097/WCO.0b013e328305bdaf.

Carpenter, M.G., Allum, J.H., Honegger, F., 2001. Vestibular influences on human postural control in combinations of pitch and roll planes reveal differences in spatiotemporal processing. Exp. Brain Res. 140 (1), 95–111. https://doi.org/10.1007/s002210100802.

Chen, J., Palmer, S.J., Khan, A.R., McKeown, M.J., Beg, M.F., 2009. Freesurfer-initialized large deformation diffeomorphic metric mapping with application to Parkinson's disease. Proc SPIE 2009; 7259, Medical Imaging 2009: Image Processing, 725931. doi:10.1117/12.810854.

Crouse, J.J., Phillips, J.R., Jahanshahi, M., Moustafa, A.A., 2016. Postural instability and falls in Parkinson's disease. [Review]. Rev. Neurosci. 27 (5), 549–555. https://doi.org/10.1515/revneuro-2016-0002.

de Lima-Pardini, A.C., de Azevedo Neto, R.M., Coelho, D.B., Boffino, C.C., Shergill, S.S., de Oliveira, Souza C., et al., 2017. An fMRI-compatible force measurement system for the evaluation of the neural correlates of step initiation. Sci. Rep. 7, 43088. https://doi.org/10.1038/srep43088.

Domingos, J.M., Godinho, C., Dean, J., Coelho, M., Pinto, A., Bloem, B.R., et al., 2015. Cognitive Impairment in Fall-Related Studies in Parkinson's Disease. [Review]. J Parkinsons Dis 5 (3), 453–469. https://doi.org/10.3233/JPD-150590.

Fasano, A., Canning, C.G., Hausdorff, J.M., Lord, S., Rochester, L., 2017. Falls in Parkinson's disease: A complex and evolving picture. [Review]. Mov. Disord. 32 (11), 1524–1536. https://doi.org/10.1002/mds.27195.

Ferraye, M.U., Debû, B., Heil, L., Carpenter, M., Bloem, B.R., Toni, I., 2014. Using motor imagery to study the neural substrates of dynamic balance. PLoS ONE 9 (3). https://doi.org/10.1371/journal.pone.0091183.

Filippi, M., Elisabetta, S., Piramide, N., Agosta, F., 2018. Functional MRI in Idiopathic Parkinson's Disease. [Review]. Int. Rev. Neurobiol. 141, 439–467. https://doi.org/10.1016/bs.irn.2018.08.005.

Filyushkina, V., Popov, V., Medvednik, R., Ushakov, V., Batalov, A., Tomskiy, A., et al., 2019. Hyperactivity of Basal Ganglia in Patients With Parkinson's Disease During Internally Guided Voluntary Movements. Front. Neurol. 10, 847. https://doi.org/10.3389/fneur.2019.00847.

Friston, K.J., 2011. Functional and effective connectivity: a review. [Review]. Brain. Connect 1 (1), 13–36. https://doi.org/10.1089/brain.2011.0008.

Gilat, M., Dijkstra, B.W., D'Cruz, N., Nieuwboer, A., Lewis, S.J.G., 2019. Functional MRI to Study Gait Impairment in Parkinson's Disease: a Systematic Review and Exploratory ALE Meta-Analysis. [Review]. Curr. Neurol. Neurosci. Rep. 19 (8), 49. https://doi.org/10.1007/s11910-019-0967-2.

Goel, R., Nakagome, S., Rao, N., Paloski, W.H., Contreras-Vidal, J.L., Parikh, P.J., 2019. Fronto-Parietal Brain Areas Contribute to the Online Control of Posture during a Continuous Balance Task. Neuroscience 413, 135–153. https://doi.org/10.1016/j.neuroscience.2019.05.063.

Goetz, C.G., Poewe, W., Rascol, O., Sampaio, C., Stebbins, G.T., Counsell, C., et al., 2004. Movement Disorder Society Task Force report on the Hoehn and Yahr staging scale: status and recommendations. Mov. Disord. 19 (9), 1020–1028. https://doi.org/10.1002/mds.20213. PMID: 15372591.

Goetz, C.G., Tilley, B.C., Shaftman, S.R., Stebbins, G.T., Fahn, S., Martinez-Martin, P., et al., 2008. Movement Disorder Society-sponsored revision of the Unified Parkinson's Disease Rating Scale (MDS-UPDRS): scale presentation and clinimetric testing results. Mov. Disord. 23 (15), 2129–2170. https://doi.org/10.1002/mds.22340.

Grimbergen, Y.A., Langston, J.W., Roos, R.A., Bloem, B.R., 2009. Postural instability in Parkinson's disease: the adrenergic hypothesis and the locus coeruleus. [Review]. Expert Rev. Neurother. 9 (2), 279–290. https://doi.org/10.1586/14737175.9.2.279.

Guillot, A., Di Rienzo, F., Macintyre, T., Moran, A., Collet, C., 2012. Imagining is Not Doing but Involves Specific Motor Commands: A Review of Experimental Data Related to Motor Inhibition. [Review]. Front. Hum. Neurosci. 6, 247. https://doi.org/10.3389/fnhum.2012.00247.

Indovina, I., Riccelli, R., Chiarella, G., Petrolo, C., Augimeri, A., Giofrè, L., et al., 2015. Role of the Insula and Vestibular System in Patients with Chronic Subjective Dizziness: An fMRI Study Using Sound-Evoked Vestibular Stimulation. Front. Behav. Neurosci. 9, 334. https://doi.org/10.3389/fnbeh.2015.00334.

Jacobs, J.V., Horak, F.B., 2007. Cortical control of postural responses. [Review]. J. Neural Transm. (Vienna) 114 (10), 1339–1348. https://doi.org/10.1007/s00702-007-0657-0.

Jahn, K., Deutschländer, A., Stephan, T., Strupp, M., Wiesmann, M., Brandt, T., 2004. Brain activation patterns during imagined stance and locomotion in functional magnetic resonance imaging. Neuroimage 22 (4), 1722–1731. https://doi.org/10.1016/j.neuroimage.2004.05.017.

Jahn, K., Deutschländer, A., Stephan, T., Kalla, R., Wiesmann, M., Strupp, M., et al., 2008. Imaging human supraspinal locomotor centers in brainstem and cerebellum. Neuroimage 39 (2), 786–792. https://doi.org/10.1016/j.neuroimage.2007.09.047.

Kalicinski, M., Kempe, M., Bock, O., 2015. Motor imagery: effects of age, task complexity, and task setting. Exp. Aging Res. 41 (1), 25–38. https://doi.org/10.1080/0361073X.2015.978202.

Karim, H.T., Sparto, P.J., Aizenstein, H.J., Furman, J.M., Huppert, T.J., Erickson, K.I., et al., 2014. Functional MR imaging of a simulated balance task. Brain Res. 1555, 20–27. https://doi.org/10.1016/j.brainres.2014.01.033.

Katschnig, P., Schwingenschuh, P., Jehna, M., Svehlík, M., Petrovic, K., Ropele, S., et al., 2011. Altered functional organization of the motor system related to ankle movements in Parkinson's disease: insights from functional MRI. J. Neural. Transm. (Vienna) 118 (5), 783–793. https://doi.org/10.1007/s00702-011-0621-x.

Kim, S.D., Allen, N.E., Canning, C.G., Fung, V.S., 2013. Postural instability in patients with Parkinson's disease. Epidemiology, pathophysiology and management. [Review]. CNS Drugs 27 (2), 97–112. https://doi.org/10.1007/s40263-012-0012-3.

Li, J., Wang, Z.J., McKeown, M.J., 2006. Dynamic Bayesian networks (DBNS) demonstrate impaired brain connectivity during performance of simultaneous movements in Parkinson's disease. In: Biomedical Imaging: Nano to Macro. 3rd IEEE International Symposium 2006, pp. 964–967. https://doi.org/10.1109/ISBI.2006.1625080.

Li, J., Wang, Z.J., McKeown, M.J., 2007. A Multi-Subject, Dynamic Bayesian Networks (DBNS) Framework for Brain Effective Connectivity. In: IEEE conference on Acoustics, Speech and Signal Processing - ICASSP, pp. I-429–I-432.

Li, J., Wang, Z., McKeown, M.J., 2008a. Learning brain connectivity with the false-discovery-rate-controlled PC-algorithm. Conf. Proc. IEEE Eng. Med. Biol. Soc. 2008, 4617–4620. https://doi.org/10.1109/IEMBS.2008.4650242.

Li, J., Wang, Z.J., Palmer, S.J., McKeown, M.J., 2008b. Dynamic Bayesian network modeling of fMRI: a comparison of group-analysis methods. Neuroimage 41 (2), 398–407. https://doi.org/10.1016/j.neuroimage.2008.01.068.

Li, J., Wang, Z.J., 2009. Controlling the False Discovery Rate of the Association/Causality Structure Learned with the PC Algorithm. J. Mach. Learn Res. 10, 475–514.

Li, H., Jia, X., Qi, Z., Fan, X., Ma, T., Ni, H., et al., 2017. Altered Functional Connectivity of the Basal Nucleus of Meynert in Mild Cognitive Impairment: A Resting-State fMRI Study. Front. Aging Neurosci. 9, 127. https://doi.org/10.3389/fnagi.2017.00127.

MacKinnon, C.D., 2018. Sensorimotor anatomy of gait, balance, and falls. In: Day BL, Lord SR, editors. Handbook of Clinical Neurology, Vol. 159 (3rd series), Balance, Gait, and Falls. Amsterdam: Elsevier B.V.; 2018. p. 3-26. doi:10.1016/B978-0-444-63916-5.00001-X.

Malouin, F., Richards, C.L., Jackson, P.L., Dumas, F., Doyon, J., 2003. Brain activations during motor imagery of locomotor-related tasks: a PET study. Hum. Brain Mapp. 19 (1), 47–62. https://doi.org/10.1002/hbm.10103.

Marinelli, L., Quartarone, A., Hallett, M., Frazzitta, G., Ghilardi, M.F., 2017. The many facets of motor learning and their relevance for Parkinson's disease. Clin. Neurophysiol. 128 (7), 1127–1141. https://doi.org/10.1016/j.clinph.2017.03.042.

Marlin, A., Mochizuki, G., Staines, W.R., McIlroy, W.E., 2014. Localizing evoked cortical activity associated with balance reactions: does the anterior cingulate play a role? J. Neurophysiol. 111 (12), 2634–2643. https://doi.org/10.1152/jn.00511.2013.

Masdeu, J.C., Gorelick, P.B., 1988. Thalamic astasia: inability to stand after unilateral thalamic lesions. Ann. Neurol. 23 (6), 596–603. https://doi.org/10.1002/ana.410230612.

Matar, E., Shine, J.M., Gilat, M., Ehgoetz Martens, K.A., Ward, P.B., Frank, M.J., et al., 2019. Identifying the neural correlates of doorway freezing in Parkinson's disease. Hum. Brain Mapp. 40 (7), 2055–2064. https://doi.org/10.1002/hbm.24506.

Mayka, M.A., Corcos, D.M., Leurgans, S.E., Vaillancourt, D.E., 2006. Three-dimensional locations and boundaries of motor and premotor cortices as defined by functional brain imaging: a meta-analysis. Neuroimage 31 (4), 1453–1474. https://doi.org/10.1016/j.neuroimage.2006.02.004.

McCall, A.A., Miller, D.M., Yates, B.J., 2017. Descending Influences on Vestibulospinal and Vestibulosympathetic Reflexes. Front. Neurol. 8, 112. https://doi.org/10.3389/fneur.2017.00112.

Melroy, S., Bauer, C., McHugh, M., Carden, G., Stolin, A., Majewski, S., et al., 2017. Development and Design of Next-Generation Head-Mounted Ambulatory Microdose Positron-Emission Tomography (AM-PET) System. Sensors (Basel) 17 (5), 1164. https://doi.org/10.3390/s17051164.

Mierau, A., Hülsdünker, T., Strüder, H.K., 2015. Changes in cortical activity associated with adaptive behavior during repeated balance perturbation of unpredictable timing. Front. Behav. Neurosci. 9, 272. https://doi.org/10.3389/fnbeh.2015.00272.

Mihara, M., Miyai, I., Hatakenaka, M., Kubota, K., Sakoda, S., 2008. Role of the prefrontal cortex in human balance control. Neuroimage 43 (2), 329–336. https://doi.org/10.1016/j.neuroimage.2008.07.029.

Morton, S.M., Bastian, A.J., 2004. Cerebellar control of balance and locomotion. [Review]. Neuroscientist 10 (3), 247–259. https://doi.org/10.1177/1073858404263517.

Mouthon, A., Ruffieux, J., Mouthon, M., Hoogewoud, H.M., Annoni, J.M., Taube, W., 2018. Age-Related Differences in Cortical and Subcortical Activities during Observation and Motor Imagery of Dynamic Postural Tasks: An fMRI Study. Neural Plast. 2018, 1598178. https://doi.org/10.1155/2018/1598178.

Ng, B., Abu-Gharbieh, R., McKeown, M.J., 2009. Adverse Effects of Template-based Warping on Spatial fMRI Analysis. Proc SPIE 2009; 7262: 72621Y-1 – 72621Y-12. doi:10.1117/12.811422.

Nieto-Castanon, A., Ghosh, S.S., Tourville, J.A., Guenther, F.H., 2003. Region of interest based analysis of functional imaging data. Neuroimage 19 (4), 1303–1316. https://doi.org/10.1016/s1053-8119(03)00188-5.

O'Shea, H., Moran, A., 2017. Does Motor Simulation Theory Explain the Cognitive Mechanisms Underlying Motor Imagery? A Critical Review. [Review]. Front. Hum. Neurosci. 11, 72. https://doi.org/10.3389/fnhum.2017.00072.

Ozcan, M., Baumgärtner, U., Vucurevic, G., Stoeter, P., Treede, R.D., 2005. Spatial resolution of fMRI in the human parasylvian cortex: comparison of somatosensory and auditory activation. Neuroimage 25 (3), 877–887. https://doi.org/10.1016/j.neuroimage.2004.11.037.

Palmer, S.J., Ng, B., Abugharbieh, R., Eigenraam, L., McKeown, M.J., 2009. Motor reserve and novel area recruitment: amplitude and spatial characteristics of

compensation in Parkinson's disease. Eur. J. Neurosci. 29 (11), 2187–2196. https://doi.org/10.1111/j.1460-9568.2009.06753.x.

Pasman, E.P., McKeown, M.J., Cleworth, T.W., Bloem, B.R., Inglis, J.T., Carpenter, M.G., 2019. A Novel MRI Compatible Balance Simulator to Detect Postural Instability in Parkinson's Disease. Front. Neurol. 10, 922. https://doi.org/10.3389/fneur.2019.00922.

Peterka, R.J., 2018. Sensory integration for human balance control. In: Day BL, Lord SR, editors. Handbook of Clinical Neurology, Vol. 159 (3rd series), Balance, Gait, and Falls. Amsterdam: Elsevier B.V.; 2018. p. 27-42. doi:10.1016/B978-0-444-63916-5.00002-1.

Peterson, D.S., Pickett, K.A., Duncan, R., Perlmutter, J., Earhart, G.M., 2014. Gait-related brain activity in people with Parkinson disease with freezing of gait. PLoS ONE 9 (3). https://doi.org/10.1371/journal.pone.0090634.

Power, J.D., Barnes, K.A., Snyder, A.Z., Schlaggar, B.L., Petersen, S.E., 2012. Spurious but systematic correlations in functional connectivity MRI networks arise from subject motion. Neuroimage 59 (3), 2142–2154. https://doi.org/10.1016/j.neuroimage.2011.10.018.

Saimpont, A., Malouin, F., Tousignant, B., Jackson, P.L., 2013. Motor imagery and aging. [Review]. J. Mot. Behav. 45 (1), 21–28. https://doi.org/10.1080/00222895.2012.740098.

Saimpont, A., Malouin, F., Tousignant, B., Jackson, P.L., 2015. Assessing motor imagery ability in younger and older adults by combining measures of vividness, controllability and timing of motor imagery. Brain Res. 1597, 196–209. https://doi.org/10.1016/j.brainres.2014.11.050.

Schniepp, R., Möhwald, K., Wuehr, M., 2017. Gait ataxia in humans: vestibular and cerebellar control of dynamic stability. [Review]. J. Neurol. 264 (Suppl 1), 87–92. https://doi.org/10.1007/s00415-017-8482-3.

Sipp, A.R., Gwin, J.T., Makeig, S., Ferris, D.P., 2013. Loss of balance during balance beam walking elicits a multifocal theta band electrocortical response. J. Neurophysiol. 110 (9), 2050–2060. https://doi.org/10.1152/jn.00744.2012.

Snijders, A.H., Leunissen, I., Bakker, M., Overeem, S., Helmich, R.C., Bloem, B.R., et al., 2011 Jan. Gait-related cerebral alterations in patients with Parkinson's disease with freezing of gait. Brain 134 (Pt 1), 59–72. https://doi.org/10.1093/brain/awq324.

Solis-Escalante, T., van der Cruijsen, J., de Kam, D., van Kordelaar, J., Weerdesteyn, V., Schouten, A.C., 2019. Cortical dynamics during preparation and execution of reactive balance responses with distinct postural demands. Neuroimage 188, 557–571. https://doi.org/10.1016/j.neuroimage.2018.12.045.

Takakura, H., Nishijo, H., Ishikawa, A., Shojaku, H., 2015. Cerebral Hemodynamic Responses During Dynamic Posturography: Analysis with a Multichannel Near-Infrared Spectroscopy System. Front. Hum. Neurosci. 9, 620. https://doi.org/10.3389/fnhum.2015.00620.

Takakusaki, K., 2017. Functional Neuroanatomy for Posture and Gait Control. [Review]. J. Mov. Disord. 10 (1), 1–17. https://doi.org/10.14802/jmd.16062.

Taube, W., Mouthon, M., Leukel, C., Hoogewoud, H.M., Annoni, J.M., Keller, M., 2015. Brain activity during observation and motor imagery of different balance tasks: an fMRI study. Cortex 64, 102–114. https://doi.org/10.1016/j.cortex.2014.09.022.

Teo, W.P., Goodwill, A.M., Hendy, A.M., Muthalib, M., Macpherson, H., 2018. Sensory manipulation results in increased dorsolateral prefrontal cortex activation during static postural balance in sedentary older adults: An fNIRS study. Brain Behav. 8 (10) https://doi.org/10.1002/brb3.1109.

Visser, J.E., Bloem, B.R., 2005. Role of the basal ganglia in balance control. [Review]. Neural Plast. 12 (2–3), 161–272. https://doi.org/10.1155/NP.2005.161.

Winter, D.A., Patla, A.E., Prince, F., Ishac, M., Gielo-Perczak, K., 1998. Stiffness control of balance in quiet standing. J. Neurophysiol. 80 (3), 1211–1221. https://doi.org/10.1152/jn.1998.80.3.1211.

Wu, T., Hallett, M., 2005a. The influence of normal human ageing on automatic movements. J. Physiol. 562 (Pt 2), 605–615. https://doi.org/10.1113/jphysiol.2004.076042.

Wu, T., Hallett, M., 2005b. A functional MRI study of automatic movements in patients with Parkinson's disease. Brain 128 (Pt 10), 2250–2259. https://doi.org/10.1093/brain/awh569.

Wu, T., Chan, P., Hallett, M., 2010. Effective connectivity of neural networks in automatic movements in Parkinson's disease. Neuroimage 49 (3), 2581–2587. https://doi.org/10.1016/j.neuroimage.2009.10.051.

Zwergal, A., Linn, J., Xiong, G., Brandt, T., Strupp, M., Jahn, K., 2012. Aging of human supraspinal locomotor and postural control in fMRI. Neurobiol. Aging 33 (6), 1073–1084. https://doi.org/10.1016/j.neurobiolaging.2010.09.022.